Analyst

PAPER

View Article Online
View Journal

Cite this: DOI: 10.1039/c4an01549e

Amperometric hydrogen peroxide and glucose biosensor based on $NiFe_2$/ordered mesoporous carbon nanocomposites†

Dong Xiang,*[ab] Longwei Yin,*[b] Jingyun Ma,[b] Enyan Guo,[b] Qun Li,[b] Zhaoqiang Li[b] and Kegao Liu[a]

Nanocomposites of $NiFe_x$ embedded in ordered mesoporous carbon (OMC) ($x = 0, 1, 2$) were prepared by a wet impregnation and hydrogen reduction process and were used to construct electrochemical biosensors for the amperometric detection of hydrogen peroxide (H_2O_2) or glucose. The $NiFe_2$/OMC nanocomposites were demonstrated to have a large surface area, suitable mesoporous channels, many edge-plane-like defective sites, and a good distribution of alloyed nanoparticles. The $NiFe_2$/OMC and Nafion modified glass carbon electrode (GCE) exhibited excellent electrocatalytic activities toward the reduction of H_2O_2 as well. By utilizing it as a bioplatform, GOx (glucose oxidase) cross-linked with Nafion was immobilized on the surface of the electrode for the construction of an amperometric glucose biosensor. Our results indicated that the amperometric hydrogen peroxide biosensor ($NiFe_2$/OMC + Nafion + GCE) showed good analytical performances in term of a high sensitivity of 4.29 μA mM^{-1} cm^{-2}, wide linearity from 6.2 to 42 710 μM and a low detection limit of 0.24 μM at a signal-to-noise ratio of 3 ($S/N = 3$). This biosensor exhibited excellent selectivity, high stability and negligible interference for the detection of H_2O_2. In addition, the immobilized enzyme on $NiFe_2$/OMC + Nafion + GCE, retaining its bioactivity, exhibited a reversible two-proton and two-electron transfer reaction, a fast heterogeneous electron transfer rate and an effective Michaelis–Menten constant (K'_M) (3.18 mM). The GOx + $NiFe_2$/OMC + Nafion + GCE could be used to detect glucose based on the oxidation of glucose catalyzed by GOx and exhibited a wide detection range of 48.6–12 500 μM with a high sensitivity of 6.9 μA mM^{-1} cm^{-2} and a low detection limit of 2.7 μM ($S/N = 3$). The enzymic biosensor maintained a high selectivity and stability features, and shows great promise for application in the detection of glucose.

Received 23rd August 2014
Accepted 26th October 2014

DOI: 10.1039/c4an01549e

www.rsc.org/analyst

Introduction

The application of biosensors in the detection of biomolecules at low concentrations plays a crucial role in the early diagnosis and cure of diseases.[1,2] Hydrogen peroxide (H_2O_2) is used as an oxidizing agent in biological and chemical industries.[3] It is an important intermediate oxidation product in the catalysis of glucose by glucose oxidase (GOx) in the presence of O_2 and its detection is important for the diagnosis of various diseases. Glucose is an important metabolite in living organisms, and its detection is especially important in the case of patients suffering from diabetes.[4,5] Among the methods used for detecting H_2O_2 and glucose,[6–8] electrochemical methods have proved to be attractive because of their convenience, low cost, high selectivity, and high sensitivity.[9,10] Glucose enzymatic (glucose oxidase, GOx) biosensors, in particular, have been shown to be highly selective and sensitive, are widely used and play a vital role in monitoring the blood glucose of diabetic patients.[1,11] However, some properties, including chemical and thermal instabilities, can change the activity of enzymes causing degeneration, low activity and less reproducibility.[12] The same problem arises in the detection of H_2O_2. The growing emergence of nanomaterials has provided the prerequisites for the development of electrochemical biosensors for highly sensitive, timely and accurate detection because of the extremely reduced size of nanomaterials, their large surface-to-volume ratios, and their high levels of crystallinity.[1,10] The significant focus of this research was the development of an amperometric electrochemical biosensor based on composite carbon nanomaterials.

Carbon materials have many electrochemical advantages, such as a low background current, a wide potential window, they are inert, not costly and exhibit high conductivity.[13] These

[a]School of Material Science and Engineering, Shandong Jianzhu University, Jinan 250101, P. R. China. E-mail: xiang@sdjzu.edu.cn; Tel: + 86 531 86367285

[b]Key Laboratory of Liquid-Solid Structural Evolution and Processing of Materials, Ministry of Education, School of Materials Science and Engineering, Shandong University, Jinan 250061, P. R. China. E-mail: yinlw@sdu.edu.cn; Fax: +86 531 88396970; Tel: + 86 531 88396970

† Electronic supplementary information (ESI) available. See DOI: 10.1039/c4an01549e

properties are considered to be good for analytical applications and for the electrochemical performance of electrode materials. Carbon materials used in electrochemical biosensors mainly include graphite,[14] glassy carbon,[15] carbon fibers,[16] and carbon nanotubes.[17,18] Ordered mesoporous carbon (OMC) is synthesized by the "template" method, which involves the use of ordered hexagonal and cubic mesoporous silicon or aluminum silicon as an "inorganic template".[19] OMC has been applied in catalysis, sensors, bioreactors and energy storage, *etc.*[20–27] because of its excellent properties such as its high specific surface area, tunable pore size distribution, high thermal stability, flexible structure, and electrical conductivity.[28–31] When OMC is used as a modified electrode, it can conduct electron transfer between the substrates. Jia *et al.*[32] reported that an OMC modified electrode could be used to select and detect dopamine by ascorbic acid (AA) due to its catalytic oxidation properties. Zhou *et al.*[33] found that OMC had a higher and more stable electric catalytic response for NADH (Nicotinamide Adenine Dinucleotide Health) than that of carbon nanotubes (CNTs). OMC can provide a platform for dehydrogenase-based electrochemical biosensors, which is beneficial for electrical conductivity and results in good performance of the electrochemical biosensor. Zhou *et al.*[29] reported that OMC is intrinsically a good conductor and plays an important role in electron transfer with most of its redox partners. By means of modification of its surface area, OMC has been used as a catalyst support for the fabrication of electrochemical biosensors. In addition, for the preparation of active sites, metal or metallic oxide nanoparticles, such as Pt,[34,35] Au,[36] Ag,[37] Ni,[38,39] Cu,[40] or CoO,[41] , have been embedded into OMC. Yu *et al.*[42] reported a glucose biosensor with high sensitivity based on a film of GOx with immobilized Pt nanoparticles deposited on a mesoporous carbon (CMK-3) electrode. Ndamanisha *et al.*[43] demonstrated the use of a ferrocene and mesoporous carbon composite (OMC–Fe) to make an H_2O_2 electrochemical sensor with high sensitivity and stability. Compared with pure OMC, the detection range of the OMC–Fe electrode for H_2O_2 was greater, and the reproducibility was good. In recent years, the application of monometallic electrode materials has been shown to have two fundamental problems including low efficiency and a poisoning effect due to chemisorbed intermediates.[44] Hence, nanocomposites especially metallic alloy nanoparticles (MANPs) (such as Pt–Pd, Pt–Ir, Cu–Pd, Au–Pt, and Au–Ag)[45–49] have drawn more and more attention for their potential applications in biotechnology and bioanalytical chemistry.[50,51] MANPs modified electrodes show outstanding advantages in electroanalysis such as catalysis, enhancement of mass transport, good cooperated synergy, high effective surface area, and control over the electrode microenvironment.[52,53] They often exhibit better catalytic properties than their monometallic counterparts.[48,51,54] Pandey *et al.*[55] synthesized composite materials of PB–Au(I)/AuNPs–Pd for the detection of H_2O_2 which exhibited excellent electrocatalytic behavior as well as extending the applied potential of H_2O_2 reduction towards the anodic direction. Noh *et al.*[56] were the first to report catalysts for the oxidation of glucose and the reduction of H_2O_2 by using a Cu–Co alloy dendrite, and the glucose sensor developed by them was successfully applied in the analysis of real human blood samples. The Cu–Co dendrite material can be widely used as a long-term stable catalyst for glucose and H_2O_2 sensors.

Herein, $NiFe_x$/OMC nanocomposites were prepared by a wet impregnation and hydrogen reduction method. The electrochemical biosensor electrodes including $NiFe_x$/OMC + Nafion + GCE and GOx + $NiFe_x$/OMC + Nafion + GCE, were fabricated from $NiFe_x$/OMC, Nafion, and GOx modified glass carbon electrodes (GCE). The electrochemical performance of the $NiFe_x$/OMC + Nafion + GCE was assessed for the detection of H_2O_2 in phosphate buffer solution (PBS), while the GOx + $NiFe_x$/OMC + Nafion + GCE was applied in the detection of glucose in PBS. After successive addition of H_2O_2 solution to PBS, the sensitivity of the electrode was shown to be high, the limit of detection was low and the linear detection range was wide, but the sensor failed after addition of glucose solution. When GOx was immobilized on the surface of the GCE, high electrochemical performance and stability for the detection of glucose in PBS under the action of the enzyme were maintained for the GOx + $NiFe_x$/OMC + Nafion + GCE.

Experimental

Chemical and reagents

P123 triblock copolymer, Nafion-115 ® ion-crosslinked polymer, glucose oxidase (GOx, Type X-S, 100 000 U g^{-1}), and bovine serum protein were purchased from Aldrich, DuPont, Sigma, and JieRun (China), respectively. Phosphate buffer saline (0.1 M PBS) with 9 g L^{-1} NaCl with different pH values was prepared from stock solutions of H_3PO_4, Na_2HPO_4, and NaH_2PO_4, which was used as the supporting electrolyte. The other chemicals used such as tetraethoxysilane (TEOS), sucrose, sulfuric acid (98%), hydrofluoric acid (HF, 40%), nickel acetate, iron nitrate, ethanol, hydrogen peroxide (H_2O_2, 37%), uric acid (UA, 99%), ascorbic acid (AA, 99.5%) and glucose were obtained from Sinopharm Chemical Reagent Co. Ltd (China). Glucose stock solution was stored overnight at room temperature before analysis. The stock GOx solution was prepared in the PBS buffer and stored at 277 K. Unless otherwise stated, reagents were of analytical grade and were used as received. Doubly distilled water from a Millipore system (>18 MΩ cm) was used throughout the experiments.

Apparatus and procedures

The structure, phase composition, and morphology of the as-prepared samples were investigated by X-ray diffraction (XRD, Rigaku D/max-2500, Cu K_α radiation) and transmission electron microscopy (HR-TEM, JEM-2100). Nitrogen adsorption–desorption isotherms were determined at 77 K using an adsorption porosimeter Micromeritics ASAP 2020 system. The surface area measurements were performed according to the Brunauer–Emmett–Teller (BET) method, while the pore size distribution was obtained from the adsorption branch of the isotherm by using the corrected form of the Kelvin equation by means of the Barrette Joynere Halenda (BJH) method. Raman spectra were recorded using a Horiba Jobin-Yvon microRaman spectrometer

equipped with a microscope and a 633 nm laser as the excitation source.

Electrochemical performance was assessed using a Princeton Parstate 2273A electrochemical station with a three-electrode system by using a Pt sheet as the counter electrode and an Ag/AgCl (in saturated KCl) as the reference electrode in PBS as the electrolyte. The preparation process of the working electrode was described in the sample preparation section. The geometric surface area of the prepared working electrode was about 0.071 cm^2. The electrochemical impedance spectroscopy (EIS) measurements of the samples were performed at 0 V *vs.* an open circuit potential with an excitation signal of 5 mV at a frequency range of 10 kHz–100 mHz in 0.1 M PBS solution containing 1.0 mM H_2O_2 or 1.0 mM glucose. The impedance data were fitted to an appropriate equivalent circuit using ZSimpWin 3.0 software (Echem Software). The cyclic voltammogram (CV) curves were recorded using an electrochemical station at a potential range of −1.0 to 0.5 V with different scanning rates, and amperometric measurements were also recorded of a magnetically stirred PBS solution.

Preparation of SBA-15, OMC, and $NiFe_x$/OMC

In the present work, hexagonally ordered SBA-15 was used as a template for the synthesis of OMC. The synthesis of SBA-15 was performed using the following method: P123 triblock copolymer was used as a supramolecular template and tetraethoxysilane (TEOS) was used as a silica source under near neutral conditions.[28] The hexagonally ordered OMC was replicated from the above-synthesized SBA-15 template by using sucrose as a carbon precursor. The synthesis of OMC was performed in a similar way by synthesizing CMK-3 mesoporous carbon.[29,34,35]

The $NiFe_x$ alloy embedded OMC was synthesized by adding 0.1 g of OMC to nickel acetate and iron nitrate solution (5 mg mL^{-1}). After stirring for 1 h and immersion for 12 h at room temperature, and evaporation at 353 K, a black powder was obtained which was calcined at 673 K for 2 h under a flow of nitrogen. The samples were kept in a H_2 atmosphere at 723 K for 2 h. Then, the $NiFe_x$ nanoparticles embedded OMC were obtained and labeled as Ni/OMC, NiFe/OMC, and $NiFe_2$/OMC, respectively.

Preparation of $NiFe_x$/OMC + Nafion + GCE and GOx + $NiFe_x$/OMC + Nafion + GCE

The GCE was ground stepwise with metallographic sandpaper (from 1# to 7#), then polished to a mirror finish with 1.0 and 0.3 μm Al_2O_3 slurries successively, and finally washed sequentially with ethanol and deionized water in an ultrasonic bath, the electrode surface was then dried with N_2 gas. 10 mg of $NiFe_x$/OMC catalyst and 1 mL of 0.1 M PBS solution (pH 7.0) were mixed, 25 μL of the mixed catalyst was dropped onto the GCE using a micro-syringe, the GCE was then dried at room temperature. 5 μL of 5% Nafion-115 ® ion-crosslinked polymer was mixed and dropped onto the electrode surface followed by drying at room temperature. $NiFe_x$/OMC + Nafion + GCE ($x = 0$, 1, 2) was obtained.

The $NiFe_x$/OMC + Nafion + GCE ($x = 0$, 1, 2) was prepared by repeating the above process. 10 μL of GOx solution (20 mg L^{-1}), 5 μL of bovine serum protein, and 5 μL of PBS (pH 6.5) solution were taken, and ultrasonically mixed for 10 min, then stored at 277 K in a refrigerator and kept for 24 h. The mixed droplets were dropped on the surface of the electrode. 5 μL of 5% Nafion-115 ® ionomer was plated on the electrode surface followed by drying at room temperature.

Results and discussion

Materials characterization

Fig. 1a–c show typical TEM images of $NiFe_x$/OMC samples with a molar ratio for Ni–Fe of $x = 0$, 1, 2, respectively. Fig. 1d–f present the size distribution of $NiFe_x$ nanoparticles for the $NiFe_x$/OMC samples. From Fig. 1a, 1d and 1b, 1e, it can be seen that the average size of the Ni and NiFe nanoparticles is about 8.3 nm and 6.6 nm, respectively. Fig. 1c depicts a typical TEM image of a $NiFe_2$/OMC sample, indicating that the fine $NiFe_2$ nanoparticles are homogenously distributed within the pore canals of the OMC supports. Fig. 1f presents the size distribution of $NiFe_2$ nanoparticles with an average size of 4.9 nm.

Wide-angle XRD patterns of $NiFe_2$ embedded OMC samples are shown in Fig. 2a. The peaks at 44, 51, 62, and 76 degrees correspond to the (111), (200), (210) and (220) planes of the face-centered cubic (fcc) of the $NiFe_2$ crystal structure.[57,58] The XRD pattern illustrates that only pure $NiFe_2$ alloy nanoparticles are formed during the high temperature pyrolysis process. The typical low-angle XRD pattern of the $NiFe_2$/OMC composite (Fig. 2a inset) includes three well-resolved peaks assigned to (100), (110), and (200), which correspond to the highly ordered 2D hexagonal *P6mm* space group, similar to that of the SBA-15 silica host. Among the $NiFe_x$/OMC composites, $NiFe_2$/OMC has a high BET surface area of 1209 m^2 g^{-1}, a large pore volume of 1.35 cm^3 g^{-1}, and a uniform pore size (4.29 nm) (shown in Fig. 2b inset). Fig. 2c shows the Raman spectrum of $NiFe_2$/OMC with two characteristic peaks of around 1315 cm^{-1} (D band) and 1590 cm^{-1} (G band), respectively. The integral intensity ratio of these two peaks (I_D/I_G) is 3.24, which shows that the OMC prepared here has many edge-plane-like defective sites (EDSs) and a high electrocatalytic activity.[34,35]

$NiFe_x$/OMC + Nafion + GCE detection of H_2O_2

Electrochemical impedance spectroscopy (EIS) is an effective tool for studying the interface properties of surface-modified electrodes.[29] In EIS, the semicircle diameter of EIS at high frequencies equals the electron transfer resistance (R_{ct}). The size of R_{ct} depends on the dielectric and insulating properties at the electrode/electrolyte interface. The linear part at low frequencies of the Warburg element (Z_w) relates to the kinetic and diffusion process of the electrolyte. Fig. S1† exhibits the impedance spectra of the Ni/OMC + Nafion + GCE and $NiFe_2$/OMC + Nafion + GCE as the impedance response of the system. It has been found that the diameter of the Nyquist semicircle at high frequencies decreases with an increase in the amount of Fe because of the good distribution of the $NiFe_2$ nanoparticles, the

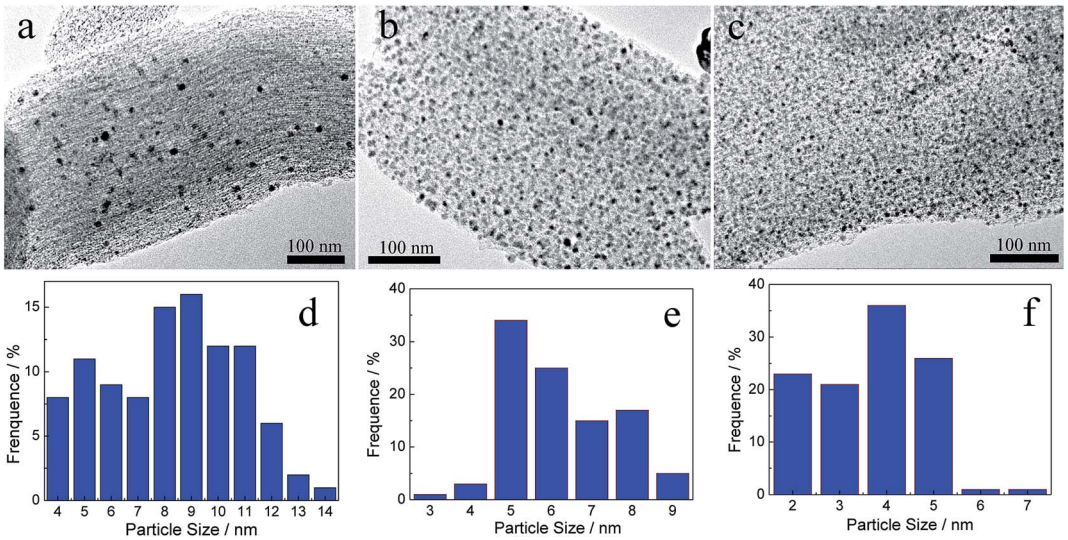

Fig. 1 TEM images and particle size distribution of $NiFe_x$/OMC, (a) Ni/OMC, (b) NiFe/OMC, (c) $NiFe_2$/OMC.

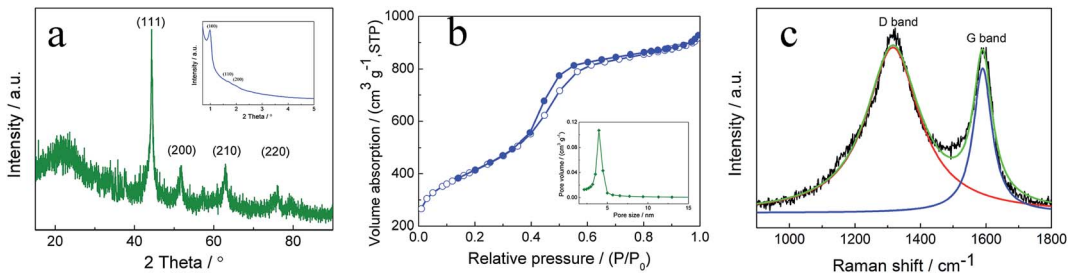

Fig. 2 (a) XRD pattern of $NiFe_2$/OMC, inset: low angle XRD of $NiFe_2$/OMC, (b) N_2 adsorption–desorption curves (open symbols: adsorption; closed symbols: desorption), inset: the pore size distribution plot for $NiFe_2$/OMC sample, (c) Raman spectra for the $NiFe_2$/OMC composite at room-temperature.

large surface area and pore volume, and the suitable pore channel of $NiFe_2$/OMC. The R_{ct} of $NiFe_2$/OMC + Nafion + GCE is 46.3 Ω cm^2. Hence, the interfacial electron transfer is improved, resulting in the decrease of the electron transfer resistance.

Cyclic voltammograms (CVs) were recorded using the OMC + Nafion+GCE and $NiFe_x$/OMC + Nafion + GCE ($x = 0, 1, 2$) for 1.0 mM H_2O_2 in 0.1 M PBS, and are shown in Fig. S2.† The redox peaks measured with the $NiFe_2$/OMC + Nafion + GCE were higher than those recorded with other electrodes. This should be helpful for its use as an electrochemical sensor material. Fig. S3† shows the CV curves of 1.0 mM H_2O_2 on $NiFe_2$/OMC + Nafion + GCE at different pH values (from 5.0 to 9.0) in 0.1 M PBS. As noted in Fig. S3a,† a pair of redox peaks was detected. When the $NiFe_2$/OMC electrode was used well-defined peaks were recorded at the redox potential for [Ni(II) and Fe(II)] to [Ni(III) and Fe (III)] (at −0.2–0 V) oxidation and an appreciable catalytic current was obtained with H_2O_2.[37,38,41] The value for the anodic peak potential (E_{pa}) shifts to a lower negative potential with an increase in pH. The peak potential of $NiFe_2$/OMC + Nafion + GCE also shows linear dependence upon the solution pH in the range from 5.0 to 9.0 with slopes of −0.0696 V pH^{-1} and −0.0375 V pH^{-1} (Fig. S3b†). The two values of the slope are close to that given by the Nernstian equation and the electrode process, therefore there appears to be an equal proton–electron transfer.[59] The experimental results also indicate that the pH value has a significant influence on the values of the anodic peak current. Maximum peak currents (i_{pa}) were observed at pH 7.0 (Fig. S3†). Considering the current intensity in the determination process of H_2O_2 and the effect of pH on the reduction potential, an optimum pH value of 7.0 was employed in the following experiments. According to the relationship between applied potential and H_2O_2 electrocatalytic reduction current, an optimum electrode potential of −0.2 V was selected for amperometric measurements in order to obtain good repeatability and high sensitivity. As shown in Fig. S3b,† the anodic peak potential value, E_{pa}, decreased to a lower negative potential with an increase of pH. This shows that higher pH values are conducive to the reduction process.[57]

To demonstrate the efficacy of the $NiFe_x$/OMC + Nafion + GCE biosensor, H_2O_2 was used for amperometric experiments *via* a three-electrode system. Fig. S4† displays the amperometric response plot (current *vs.* time, *I*–*t*) and the response of the calibration curve (current *vs.* concentration) of OMC + Nafion + GCE and $NiFe_x$/OMC + Nafion + GCE ($x = 0, 1, 2$) with successive

addition of 1.0 mM H_2O_2 steps to 0.1 M PBS (pH 7.0) with constant stirring at an applied potential of −0.20 V. All the tests involved the detection of the redox current associated with the reduction of peroxide at a working potential. As shown in Fig. S4a,† in comparison to the evident increase in the current staircases achieved with the $NiFe_x$/OMC + Nafion + GCE ($x = 0$, 1, 2), virtually no increase in the current was observed with each successive addition of H_2O_2 for a sample with pure OMC in Nafion on the surface of the electrode. When the response current of the $NiFe_x$/OMC + Nafion + GCE ($x = 0$, 1, 2) reached 95% of the steady-state current, its reaction time was 8, 6, and 5 s, respectively. Among the electrodes, $NiFe_2$/OMC + Nafion + GCE has the highest reaction rate for H_2O_2 owing to its high surface area, uniform pore size and the controllable structure of $NiFe_2$/OMC. It can be demonstrated from Fig. S4b† that the steady-state currents of $NiFe_x$/OMC + Nafion + GCE increase linearly for H_2O_2 reduction with an increase of H_2O_2 concentration. The linear regression equations are $y_1 = 0.799x_1 + 2.773$ ($R_1^2 = 0.99472$), $y_2 = 1.622x_2 + 4.963$ ($R_2^2 = 0.99292$), and $y_3 = 2.327x_3 + 6.615$ ($R_3^2 = 0.99574$), respectively. From the calibration curves, it can be calculated that the sensitivity of the $NiFe_2$/OMC + Nafion + GCE is higher than that of Ni/OMC + Nafion + GCE. The sensitivity enhancement is attributed to the small size of $NiFe_2$ nanoparticles, and those nanoparticles improve the ratio of active atoms with the increase of the sensing efficiency of H_2O_2. At the end of the biochemical reaction on the modified electrode surface H_2O_2 is oxidized to oxygen because of the addition of electrons. It has been shown that the reduction reaction of H_2O_2 occurs between OMC and $NiFe_x$ nanoparticles (Fig. S5†). Due to its catalytically active surface, OMC with $NiFe_x$ nanoparticles embedded as a mediator, influences charge transfer between the electrode and the analyte, and can promote the reduction of H_2O_2 and provide a base for the mediation of H_2O_2.[42,58] The chemical reaction process of H_2O_2 reduction is as follow:

$$H_2O_2 \rightarrow 2H^+ + O_2 + 2e^- \quad (1)$$

Fig. 3a displays the dynamic response (I–t curve) of $NiFe_2$/OMC + Nafion + GCE under the optimal experimental conditions with successive addition of different concentrations of H_2O_2 to 0.1 M PBS (pH 7.0) with stirring at −0.2 V. The current rapidly increased after the addition of H_2O_2, and a steady-state current (95% of the maximum value) was obtained within an average of 5 s, indicating a fast electron transfer rate between H_2O_2 and the modified electrode. In addition, OMC allows the rapid transport of liquid due to its porous structure and extremely high surface area, which is desirable for electrochemical reactions.[31] Fig. 3b shows the calibration curve of the response current *vs.* H_2O_2 concentration measured using the $NiFe_2$/OMC + Nafion + GCE. The linear regression equation is $y = 0.30032x + 6.469$ ($R^2 = 0.99374$). The trace clearly demonstrates the fast response and high sensitivity of the electrode to H_2O_2. The modified electrode has a good linear response to the concentration of H_2O_2 in the range from 6.2 to 42 710 μM with a sensitivity of 4.29 μA mM^{-1} cm^{-2}. The favorable amperometric signals are accompanied with a low noise level, which results in an excellent detection limit for H_2O_2. The detection limit is 0.24 μM when the signal to noise ratio is 3 ($S/N = 3$). Therefore, the $NiFe_2$/OMC + Nafion + GCE sensor has high sensitivity, a low detection limit, easy electron transition, a fast response rate and a wide detection scope for H_2O_2. Table 1 is a comparison of the homemade sensors with the data from reported literature for linear range, sensitivity and detection limit. The results show that the $NiFe_2$/OMC + Nafion + GCE exhibits an excellent electrochemical performance compared to that of other recently reported electrodes (except Fe/OMC). Thus, $NiFe_2$/OMC which is a good electrode material as an amperometric sensor for the detection of H_2O_2 has the features of low detection potential, high sensitivity, and a wide linear range.

$NiFe_2$ alloyed nanoparticles embedded in OMC can be used for the direct electrochemical detection of H_2O_2 and also as a substrate for the detection of other additives such as ascorbic acid (AA), sucrose, glucose, and uric acid (UA). Fig. 4 shows the amperometric current curve recorded using the $NiFe_2$/OMC + Nafion + GCE electrochemical biosensor for the detection of 0.5 mM H_2O_2, sucrose, glucose, AA, and UA in 0.1 M PBS (pH 7.0) solution, respectively. The additives except H_2O_2 have little effect on the performance of the modified electrode. This is because the cross-linked effects occurring in the cation exchangers of the Nafion membrane can effectively prevent the interferent from passing into the polymer film, and the electrode is not sensitive to interference.[61–63] Therefore, $NiFe_2$/OMC + Nafion + GCE biosensor has a remarkable selectivity for the determination of H_2O_2.

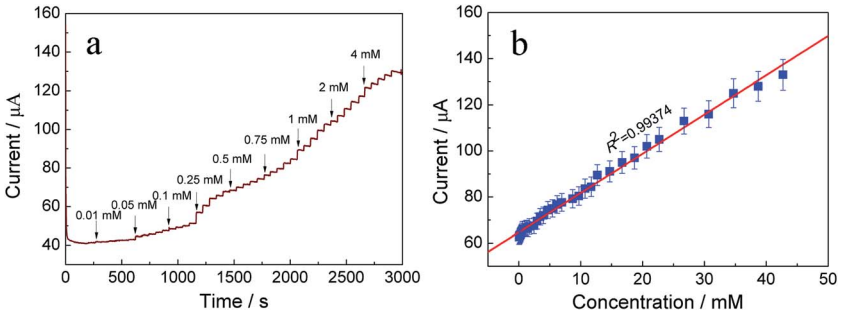

Fig. 3 (a) I–t response curve for successive addition of different H_2O_2 concentrations at $NiFe_2$/OMC + Nafion + GCE, measured in 0.1 M PBS (pH 7) solution at −0.20 V in N_2 saturated, rotation speed: 400 rpm, (b) calibration curve of response current *vs.* H_2O_2 concentration.

Table 1 Comparison of the performance of various hydrogen peroxide sensors

Electrode materials	Linear range/μM	Sensitivity/ (μA mM^{-1} cm^{-2})	Detection limit/μM	Ref.
$NiFe_2$/OMC	6.2–42 710	4.29	0.24	This work
Fe/OMC	7.0–4000	8.4	0.036	42
Pt/CNT	5.0–25 000	1.4	1.5	59
Au/CNT	0.02–300	0.11	0.4	35
P2Mo18/OMC	5.34–24 000	2.8	1.78	21
Mesoporous Pt	20–40 000	2.8	4.5	60
OMC	10–1000	1.95	2.23	12

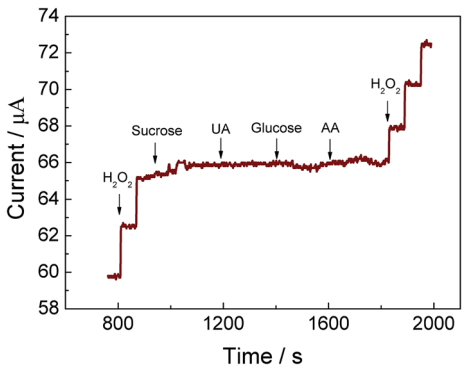

Fig. 4 Amperometric response of 0.5 mM H_2O_2, sucrose, UA, AA, and glucose at $NiFe_2$/OMC + Nafion + GCE in N_2 saturated 0.1 M PBS (pH 7), applied potential: −0.2 V, rotation speed: 400 rpm.

The current response of the $NiFe_2$/OMC + Nafion + GCE electrochemical biosensor remained mainly unchanged in 0.1 M PBS (pH 7.0) + 0.5 mM H_2O_2 for 50 consecutive scanning cycles, as can be seen from the CV. The relative standard deviation (RSD) was 3.6% for five replicates of the same measurement, suggesting that the fabrication procedure of the sensor was reliable, thereby allowing reproducible electroanalysis responses to be obtained with electrodes constructed in the same manner but with different compositions. This shows that the electrochemical biosensor electrode has good reproducibility. The long-term stability of an electrochemical biosensor is one of the most importance features for its practical application. In order to evaluate its stability, $NiFe_2$/OMC + Nafion + GCE was stored in a solution of 0.1 M PBS (pH 7.0) under ambient air conditions for 4 weeks. And every other week, its current response was obtained following the same process. The results obtained showed that there was little change in the current response. Compared with the initial value of the biosensor, the sensitivity only fell by 5% after 4 weeks, which showed that strong binding occurred between the mediator and the matrix. The mediator of $NiFe_2$/OMC + Nafion prevents the leaching of contaminants from the electron transfer reaction. Therefore, the application of the mediator provides both mechanical and chemical stability to the electrode. It means that $NiFe_2$/OMC + Nafion + GCE has good activity and stability for H_2O_2.

GOx + $NiFe_x$/OMC + Nafion + GCE detection of glucose

The Nyquist diagrams of GOx + Ni/OMC + Nafion + GCE and GOx + $NiFe_2$/OMC + Nafion + GCE were recorded at the oxidation peak potential for 1.0 mM glucose in 0.1 M PBS (pH 6.5), as shown in Fig. S6.† In the case of the above electrode materials, the diameters of their semicircles at high frequencies is related to the resistance (R_{ct}) of the charge transfer reaction and the electronic resistance of the modified film. By analyzing the linear part at the low frequency region, it can be observed that the process turns from a semi-infinite diffusion to a finite diffusion on the surfaces of GOx + Ni/OMC + Nafion + GCE and GOx + $NiFe_2$/OMC + Nafion + GCE. Compared with the diameter of the semicircle present in the high frequency region on GOx + Ni/OMC + Nafion + GCE, a lower resistance R_{ct} can be observed for GOx + $NiFe_2$/OMC + Nafion + GCE of 73.4 Ω cm^2. This phenomenon indicates that GOx immobilized on OMC with the $NiFe_2$ nanoparticles can promote the charge transfer rate.

Fig. S7† shows the CVs recorded with the GOx + OMC + Nafion + GCE and GOx + $NiFe_x$/OMC + Nafion + GCE ($x = 0, 1, 2$) for 1.0 mM glucose in 0.1 M PBS. GOx + $NiFe_2$/OMC + Nafion + GCE has the highest redox peaks. The CVs and the relation plots of potential E_{pa} *vs.* current I_{pa} were tested in a solution of 1.0 mM glucose and 0.1 M PBS at different pH values (6.0–8.0) of GOx + $NiFe_2$/OMC + Nafion + GCE (shown in Fig. S8a†). A pair of oxidation and reduction peaks for each electrode were present between −0.5 and 0.2 V, and the current peak was smaller than that of $NiFe_2$/OMC + Nafion + GCE. In addition, the redox peaks shifted toward the positive potential because of the glucose oxidation–reduction reaction on GOx. Fig. S8b† shows the linear relationship between potentials and pH values. The slope of the line was determined to be −0.0604 V pH^{-1}, which is close to that reported in the literature (the GOx ($FADH_2$) conversion reaction theoretical value of −59 mV pH^{-1}). This illustrates that this is a two-electron, two-proton (2e, 2H) reaction process.[63–65] At a pH value of 6.5, the maximum current value I_{pa} was attained. Accordingly, a solution pH value of 6.5 was used in subsequent experiments. It should be noted that 0.2 V was selected because such an applied potential would be beneficial to decrease the background current and minimize the responses of common interference species.

Due to its excellent analytical performance for the detection of H_2O_2, biorecognition species such as enzymes immobilized on $NiFe_x$/OMC + Nafion + GCE were further explored as

platforms for the construction of biosensors. The biosensors were prepared by anchoring GOx on the $NiFe_x$/OMC *via* cross linking with Nafion. Typically, the current response of GOx + $NiFe_x$/OMC + Nafion + GCE was in accordance with the electrocatalytic reaction of GOx molecules for successive addition of 0.5 mM glucose to 0.1 M PBS (pH 6.5) solution with continuous stirring at 0.2 V (shown in Fig. S9a†). Glucose biosensor was accomplished in the same electroanalytical procedures as in the experiments of H_2O_2. The intermediate product of H_2O_2 can directly be generated by the electrooxidation reaction occuring on the enzymatic reaction of GOx + $NiFe_x$/OMC + Nafion + GCE for glucose, which is proportional to the glucose concentration. Fig. S9b† shows that the linear calibration curves of regression equations of GOx + $NiFe_x$/OMC + Nafion + GCE ($x = 0, 1, 2$) are $y_4 = -0.06521x_4 - 0.2325$ ($R_4{}^2 = 0.99286$), $y_5 = -0.13435x_5 - 0.269$ ($R_5{}^2 = 0.99426$), and $y_6 = -0.32515x_6 - 0.5575$ ($R_6{}^2 = 0.99613$), respectively. It can be calculated that GOx + $NiFe_2$/OMC + Nafion + GCE has not only a high sensitivity, but also a fast response to glucose.

In order to assess the biological activity of GOx immobilized on the surface of the biosensor, the Michaelis–Menten constant (K'_M) is determined by the current changes by using the Lineweaver–Burk-type formula (shown in formula (1)).[66]

$$\frac{1}{i_{ss}} = \left(\frac{K'_M}{i_{max}}\right)\left(\frac{1}{C}\right)\left(\frac{1}{i_{max}}\right) \quad (2)$$

Where i_{ss} is the steady-state current of the given concentration (C), i_{max} is the maximum testing current when the analyte is saturated. The effective Michaelis–Menten constant (K'_M) of GOx + $NiFe_2$/OMC + Nafion + GCE biosensor is 3.18 mM calculated from Fig. 5a, which is inferior to CNT-based biosensor of 8.2 mM,[67] glucose at the GOx/Pt/Fe_yO_x–MWCNTs/CS of 9 mM,[52] the glucose sensor (GOx–GCE) fabricated by sol-gel of 22 and 23 mM,[65,68] and GOx in a glucose sensor of 15.7 mM.[69] Assumed that the rate of the enzymatic reaction is controlled by the quality of the transmission,[69] then, the lower Michaelis–Menten constant is related to the sensitivity and detection limit, and it can be considered that the GOx + $NiFe_2$/OMC + Nafion + GCE generates a unique microenvironment of enzymic biosensor. Thus, the prepared electrode of GOx + $NiFe_2$/OMC + Nafion + GCE exhibits high affinity for glucose, and GOx immobilized on OMC maintains a high enzymic activity. It can be seen from Fig. 5b that the linear regression equation of low concentration is $y' = -0.49014x' - 0.12929$ ($R^2 = 0.99715$). Under the low concentration of glucose, $NiFe_2$/OMC + Nafion + GCE immobilized by active GOx has a high detection sensitivity (6.90 μA mM^{-1} cm^{-2}), a wide linear detection range (from 48.6 to 12 500 μM), and a low detection limit (2.7 μM ($S/N = 3$)). Compared with pure OMC, $NiFe_x$ nanoparticles embedded OMC is ideal promote body for electron transfer, particularly in the low concentration levels of additives. The lower noise and higher detection sensitivity can be obtained by the biosensor. In addition, GOx + $NiFe_2$/OMC + Nafion modified electrode responses to glucose more quickly, whose current reaches to 95% of steady-state current within 6 s. Compared with glucose electrochemical biosensor recently reported (Table 2), the $NiFe_2$ nanoparticles embedded OMC has a higher biocatalytic performance, and the self-control biosensor for glucose has a more sensitive response and a lower detection limit.

The possible interferences at the modified electrode have also been investigated and the results are shown in Fig. 6. Selectivity is an important assessment indicator of the application of an electrochemical biosensor. 0.5 mM of glucose, AA, UA, and sucrose solution were added to 0.1 M PBS (pH 6.5) and the current response was studied. The results show that AA solution significantly enhances the current response signals, whereas for the remaining interferents (UA, sucrose) there were no obvious current response signals. Therefore, for practical application of the GOx + $NiFe_2$/OMC + Nafion + GCE electrochemical biosensor it is necessary to minimize contact with AA.

A redox reaction drawing of glucose on the enzymic electrode is shown in Fig. 7. OMC with embedded $NiFe_x$ nanoparticles can be used as an electron transfer relaying medium (MED or M) for shortening the electron transfer distance between the center of the enzyme redox and the electrode surface,thereby creating synergy with OMC for accelerating the electron transfer rate and improving the electrocatalytic performance. Furthermore, due to their high specific surface area, OMC composite materials have a great adsorption capacity for active materials and

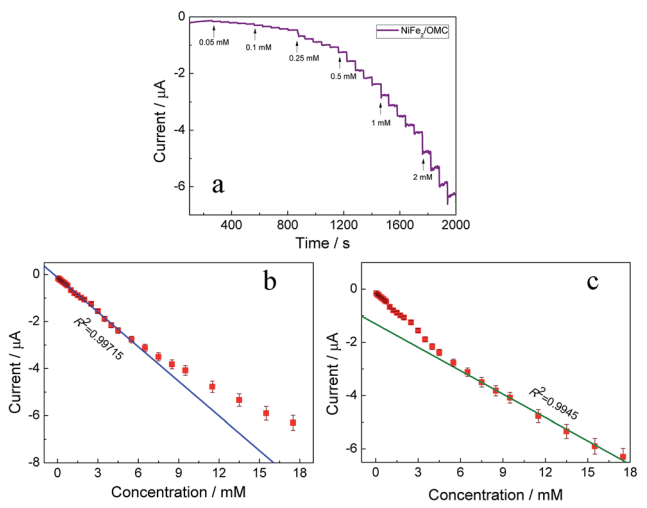

Fig. 5 (a) *I–t* response curve for successive addition of different glucose concentrations at GOx + $NiFe_2$/OMC + Nafion + GCE, measured in 0.1 M PBS pH 6.5 solution at 0.20 V, rotation speed: 400 rpm, (b) calibration curves of response current *vs.* glucose concentration at low concentration and at high concentration.

Table 2 Comparison of the performance of various glucose sensors

Electrode materials	Linear range/μM	Sensitivity/μA mM^{-1} cm^{-2}	Detection limit/μM	Ref.
GOx + $NiFe_2$/OMC	48.6–12 500	6.90	2.7	This work
GOx/Pt/OMC	40–12 200	1.79	10	41
GOx/OMC	53–15 000	0.018	72	12
GOx + Pt/CNT	160–11 500	1.28	55	59
GOx/OMC/Au	50–20 000	4.34	12	70

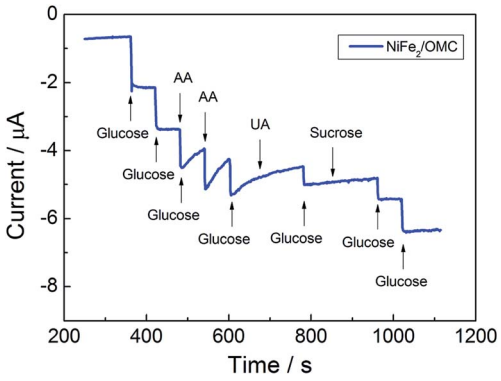

Fig. 6 Amperometric response of 0.5 mM glucose, sucrose, UA, AA at a GOx + $NiFe_2$/OMC + Nafion + GCE in N_2 saturated 0.1 M PBS (pH 6.5), applied potential: 0.2 V, rotation speed: 400 rpm.

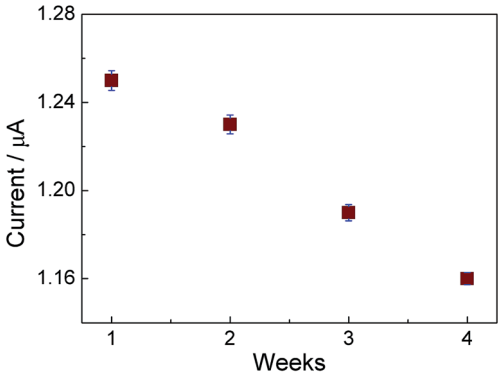

Fig. 8 Stability over 4 weeks of the amperometric response of GOx + $NiFe_2$/OMC + Nafion + GCE for the detection of 0.5 mM glucose in 0.1 M PBS solution.

increase the chance of contact with glucose. GOx + $NiFe_2$/OMC + Nafion + GCE could be used to detect glucose based on the consumption of O_2 during the oxidation of glucose catalyzed by GOx. The by product of glucose oxidation reaction is H_2O_2 (Fig. 7b). The reduction effect of $NiFe_x$ nanoparticles on H_2O_2 is very strong, which greatly enhances the electrocatalytic properties and electrical conductivity coupled with the synergistic effect, and can provide channels for the promotion of electron transfer between the $NiFe_x$/OMC and the electrode. This finally results in enhancement of the effect of the electric sensing. If the glucose oxidase as redox centers were deep in the protein shell, it is difficult to achieve the reaction of direct electron transfer in the normal electrode. This challenge can be overcome while the glucose oxidase is immobilized on matrix such as CNT, OMC, and graphene.[71,72] A good electrical activity and large specific surface area of $NiFe_x$ nanoparticles embedded OMC after the immobilization GOx can be used to effectively promote the electron transfer between the enzyme and the electrode. While a higher amount of $NiFe_x$/OMC is obtained, the glucose oxidase molecules exhibit the behavior of direct electron transfer.[5,63,73]

Additionally, the current response of the biosensor has unchanged after 50 laps continuous cyclic voltammetry in 0.1 M PBS (pH 6.5) and 0.5 mM glucose solution, showing its high reproducibility. The relative standard deviation (RSD) is 5.3% after the same five tests. The electrodes are not poisoned by the oxidation products and can be used repeatedly for the detection of glucose. In order to evaluate the stability of glucose biosensor, we made the investigation through the amperometric response to 0.5 mM glucose in 0.1 M PBS at intervals over several days, and then stored the electrode in a solution of 0.1 M PBS (pH 6.5) at 277 K. After 4 weeks, the current response was essentially constant after the same scan. Compared with the initial value of the sensitivity of the sensor, the sensitivity dropped only 7%, showing the long-term stability and good biocompatibility of GOx + $NiFe_2$/OMC + Nafion + GCE for glucose, shown in Fig. 8. It means that the enzymic glucose biosensor possesses a good superiority in terms of biological activity, sensitivity, selectivity and stability.

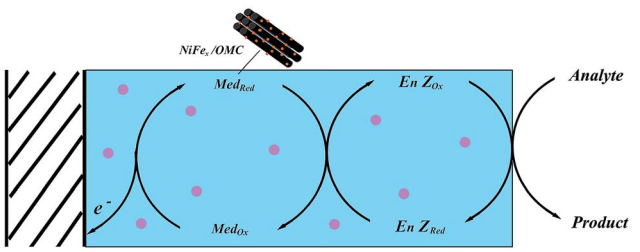

Fig. 7 (a) Redox reaction drawing of glucose biosensors-mediated on enzyme, (b) the reaction process between glucose and GOx + $NiFe_2$/OMC + Nafion + GCE.

Conclusions

$NiFe_x$/OMC nanocomposites were successfully fabricated by a wet impregnation and hydrogen reduction process. The nanocomposites of well-dispersed $NiFe_x$ nanoparticles embedded in OMC have a large surface area, suitable mesoporous channels, and many edge-plane-like defective sites. $NiFe_x$/OMC + Nafion + GCE and GOx + $NiFe_x$/OMC + Nafion + GCE electrochemical biosensors composed of $NiFe_x$/OMC, GOx, and Nafion on GCE, respectively, were prepared and used in PBS. $NiFe_2$/OMC used as electrochemical biosensor electrode materials exhibit a better quasi-reversible reaction and low electron transfer resistance (R_{ct}). When different concentrations of H_2O_2 were added to 0.1 M PBS (pH 7.0), the $NiFe_2$/OMC + Nafion + GCE was shown to have excellent electrochemical reduction activity for H_2O_2, with a high sensitivity of 4.29 μA mM^{-1} cm^{-2}, a wide detection range from 6.2 to 42 710 μM and a low detection limit of 0.24 μM ($S/N = 3$). Furthermore, the GOx + $NiFe_2$/OMC + Nafion + GCE demonstrates great electrochemical oxidation effects for glucose. The glucose biosensor had good analytical characteristics such as a wide detection range from 48.6 to 12 500 μM with a high sensitivity of 6.9 μA mM^{-1} cm^{-2}, a low detection limit of 2.7 μM ($S/N = 3$) and a low Michaelis–Menten constant ($K'_M = 3.18$ mM). These results were attributed to the direct electron transfer process occuring between the mediator (or GOx) and the electrodes because of the large specific area of OMC and the catalytic activity of the $NiFe_2$ nanoparticles. The

$NiFe_2$/OMC + Nafion + GCE and GOx + $NiFe_2$/OMC + Nafion + GCE display high sensitivity, good stability and acceptable reproducibility.

Acknowledgements

We acknowledge support from the National Natural Science Funds for Distinguished Young Scholars (51025211), National Nature Science Foundation of China (nos. 50872071 and 50972079), the Shandong Natural Science Fund for Distinguished Young Scholars (JQ200915), the Nature Science Foundation of Shandong Province (Y2007F03 and Y2008F26), the Foundation of Outstanding Young Scientists in Shandong Province (no. 2006BS04030), the Tai Shan Scholar Foundation of Shandong Province, and the Gong Guan Foundation of Shandong Province (2008GG10003019).

Notes and references

1 J. C. Claussen, A. D. Franklin, A. UlHaque, D. M. Porterfield and T. S. Fisher, *ACS Nano*, 2009, **3**, 37.
2 T. G. Drummond, *Nat. Biotechnol.*, 2003, **21**, 1192.
3 S. Chen, R. Yuan, Y. Chai and F. Hu, *Microchim. Acta*, 2013, **180**, 15.
4 X. H. Kang, Z. B. Mai, X. Y. Zou, P. X. Cai and J. Y. Mo, *Anal. Biochem.*, 2007, **369**, 71.
5 J. Luo, H. Zhang, S. Jiang, J. Jiang and X. Liu, *Microchim. Acta*, 2012, **177**, 485.
6 Y. F. Zheng, G. W. Xu, D. Y. Liu, J. H. Xiong, P. D. Zhang, C. Zhang, Q. Yang and S. Lv, *Electrophoresis*, 2002, **23**, 4104.
7 S. Hanaoka, J. M. Lin and M. Yamada, *Anal. Chim. Acta*, 2001, **426**, 57.
8 A. Lupu, P. Lisboa, A. Valsesia, P. Colpo and F. Rossi, *Sens. Actuators, B*, 2009, **137**, 56.
9 J. Xuan, L. P. Jiang and J. J. Zhu, *Chin. J. Anal. Chem.*, 2010, **38**, 513.
10 G. Wang, X. He, L. Wang, A. Gu, Y. Huang, B. Fang, B. Geng and X. Zhang, *Microchim. Acta*, 2013, **180**, 161.
11 B. J. Wang, S. Q. Gu, Y. P. Ding, Y. L. Chu, Z. Zhang, X. Ba, Q. L. Zhang and X. X. Li, *Analyst*, 2012, **138**, 362.
12 Y. F. Yang and S. L. Mu, *J. Electroanal. Chem.*, 1997, **432**, 71.
13 L. D. Zhu, C. Y. Tian, D. X. Zhu and R. L. Yang, *Electroanalysis*, 2008, **20**, 1128.
14 N. Pena, G. Ruiz, J. Reviejo and J. M. Pingarron, *Anal. Chem.*, 2001, **73**, 1190.
15 D. Z. Sun, L. D. Zhu and G. Y. Zhu, *Anal. Chim. Acta*, 2006, **564**, 243.
16 A. Schulte and R. H. Chow, *Anal. Chem.*, 1996, **68**, 3054.
17 H. X. Luo, Z. J. Shi, N. Q. Li, Z. N. Gu and Q. K. Zhuang, *Anal. Chem.*, 2001, **73**, 915.
18 J. Wang, G. Chen, M. P. Chatrathi and M. Musameh, *Anal. Chem.*, 2004, **76**, 298.
19 R. Ryoo, S. H. Joo, S. M. Kruk and S. Jun, *J. Phys. Chem. B*, 1999, **103**, 7743.
20 M. Hartmann, *Chem. Mater.*, 2005, **17**, 4577.
21 M. Zhou, J. Ding, L. P. Guo and Q. K. Shang, *Anal. Chem.*, 2007, **79**, 5328.
22 M. Zhou, L. P. Guo, F. Y. Lin and H. X. Liu, *Anal. Chim. Acta*, 2007, **587**, 124.
23 L. D. Zhu, C. Y. Tian, D. X. Zhu, X. Y. Jiang and R. L. Yang, *Electroanalysis*, 2008, **20**, 2518.
24 J. Bai, X. X. Bo, B. Qi and L. P. Guo, *Electroanalysis*, 2010, **22**, 1750.
25 J. Bai, B. Qi, C. Ndamanisha and L. P. Guo, *Microporous Mesoporous Mater.*, 2009, **119**, 193.
26 X. Bo, J. Bai, L. Wang and L. Guo, *Talanta*, 2010, **81**, 339.
27 L. Liu, L. P. Guo, X. J. Bo, J. Bai and X. J. Cui, *Anal. Chim. Acta*, 2010, **673**, 88.
28 A. Vinu, M. Miyahara and K. Ariga, *J. Phys. Chem. B*, 2005, **109**, 6436.
29 H. Zhou, S. Zhu, M. Hibino and I. Honma, *J. Power Sources*, 2003, **122**, 219.
30 C. D. Liang and S. Dai, *J. Am. Chem. Soc.*, 2006, **128**, 5316.
31 Y. F. Zhang, X. J. Bo, A. Nsabimana, C. Luhana, G. Wang, H. Wang, M. Li and L. P. Guo, *Biosens. Bioelectron.*, 2014, **53**, 250.
32 N. Jia, Z. Wang, G. Yang, H. Shen and L. Zhu, *Electrochem. Commun.*, 2007, **9**, 233.
33 M. Zhou, L. Shang, B. L. Li, L. J. Huang and S. J. Dong, *Electrochem. Commun.*, 2008, **10**, 859.
34 M. R. Guascito, E. Filippo, C. Malitesta, D. Manno, A. Serra and A. Turco, *Biosens. Bioelectron.*, 2008, **24**, 1063.
35 X. Y. Jiang, Y. H. Wu, X. Y. Mao, X. J. Cui and L. D. Zhu, *Sens. Actuators, B*, 2011, **153**, 158.
36 H. Rajabzade, P. Daneshgar, E. Tazikeh and R. Z. Mehrabian, *J. Chem.*, 2012, **9**, 2540.
37 C. M. Welch, C. E. Banks, A. O. Simm and R. G. Compton, *Anal. Bioanal. Chem.*, 2005, **382**, 12.
38 I. Danaee, M. Jafarian, F. Forouzandeh, F. Gobal and M. G. Mahjani, *Electrochim. Acta*, 2008, **53**, 6602.
39 L. M. Lu, L. Zhang, F. L. Qu, H. X. Lu, X. B. Zhang, Z. S. Wu, S. Y. Huan, Q. A. Wang, G. L. Shen and R. Q. Yu, *Biosens. Bioelectron.*, 2009, **25**, 218.
40 X. M. Miao, R. Yuan, Y. Q. Chai, Y. T. Shi and Y. Y. Yuan, *J. Electroanal. Chem.*, 2008, **612**, 157.
41 W. Z. Jia, M. Guo, Z. Zheng, T. Yu, E. G. Rodriguez, Y. Wang and Y. Lei, *J. Electroanal. Chem.*, 2009, **625**, 27.
42 J. Yu, D. Yu, T. Zhao and B. Zeng, *Talanta*, 2008, **74**, 1586.
43 J. C. Ndamanisha, Y. Hou, J. Bai and L. P. Guo, *Electrochim. Acta*, 2009, **54**, 3935.
44 L. Meng, J. Jin, G. Yang, T. Lu, H. Zhang and C. Cai, *Anal. Chem.*, 2009, **81**, 7271.
45 K. J. Chen, K. Chandrasekara Pillai, J. Ricka, C. J. Pan, S. H. Wang, C. C. Liu and B. J. Hwang, *Biosens. Bioelectron.*, 2012, **33**, 120.
46 N. A. Grace and K. Pandian, *Electrochem. Commun.*, 2006, **8**, 1340.
47 J. Luo, P. N. Njoki, Y. Lin, D. Mott, L. Y. Wang and Z. Jian, *Langmuir*, 2006, **22**, 2892.
48 C. C. Yang, A. S. Kumar, M. C. Kuo, S. H. Chien and J. M. Zen, *Anal. Chim. Acta*, 2005, **554**, 66.
49 S. Devarajan, P. Bera and S. Sampath, *J. Colloid Interface Sci.*, 2005, **290**, 117.

50 Y. Li, J. J. Zhang, J. Xuan, L. P. Jiang and J. J. Zhu, *Electrochem. Commun.*, 2010, **12**, 777.
51 X. Cui, Z. Li, Y. Yang, W. Zhang and Q. Wang, *Electroanalysis*, 2008, **20**, 970.
52 C. M. Welch and R. G. Compton, *Anal. Bioanal. Chem.*, 2006, **384**, 601.
53 X. Kang, Z. Mai, X. Zou, P. Cai and J. Mo, *Anal. Biochem.*, 2007, **363**, 143.
54 U. Yogeswaran, S. Thiagarajan and S. M. Chen, *Anal. Biochem.*, 2007, **365**, 122.
55 P. C. Pandey and A. K. Pandey, *J. Bionanosci.*, 2012, **2**, 127.
56 H. B. Noh, K. S. Lee, P. Chandra, M. S. Won and Y. B. Shim, *Electrochim. Acta*, 2012, **61**, 36.
57 K. V. P. M. Shafi, A. Gedanken, R. B. Goldfarb and I. Felner, *J. Appl. Phys.*, 1997, **81**(10), 6901–6905.
58 S. H. Kima, H. J. Sohna, Y. C. Jooa, Y. W. Kima, T. H. Yimb, H. Y. Leeb and T. Kang, *Surf. Coat. Technol.*, 2005, **199**, 43–48.
59 Z. H. Wen, S. Q. Ci and J. H. Li, *J. Phys. Chem. C*, 2009, **113**, 13482.
60 S. A. G. Evans, J. M. Elliott, L. M. Andrews, P. N. Bartlett, P. J. Doyle and G. Denuault, *Anal. Chem.*, 2002, **74**, 1322.
61 G. F. Wang, Y. Wei, W. Zhang, X. J. Zhang, B. Fang and L. Wang, *Microchim. Acta*, 2009, **168**, 87.
62 Y. Liu, M. Wang, F. Zhao, Z. Xu and S. Dong, *Biosens. Bioelectron.*, 2005, **21**, 984.
63 S. J. Bao, C. M. Li, J. F. Zang, X. Q. Cui, Y. Qiao and J. Guo, *Adv. Funct. Mater.*, 2008, **18**, 591.
64 S. Deng, G. Jian, J. Lei, Z. Hu and H. Ju, *Biosens. Bioelectron.*, 2009, **25**, 373.
65 S. Q. Liu and H. X. Ju, *Biosens. Bioelectron.*, 2003, **19**, 177.
66 R. A. Kamin and G. S. Wilson, *Anal. Chem.*, 1980, **52**, 1198.
67 B. Q. Wang, B. Li, Q. Deng and S. J. Dong, *Anal. Chem.*, 1998, **70**, 3170.
68 M. C. Rodriguez and G. A. Rivas, *Electroanalysis*, 1999, **11**, 558.
69 J. J. Xu and H. Y. Chen, *Anal. Chim. Acta*, 2000, **423**, 101.
70 L. Wang, J. Bai, X. Bo, X. Zhang and L. Guo, *Talanta*, 2011, **83**, 1386–1391.
71 Y. D. Zhao, W. D. Zhang, H. Chen and Q. M. Luo, *Anal. Sci.*, 2002, **18**, 939.
72 G. E. Anthony, C. H. Lei and R. H. Baughman, *Nanotechnology*, 2002, **13**, 559.
73 S. Dönmez, F. Arslan, N. Sarı, N. K. Yetim and H. Arslan, *Biosens. Bioelectron.*, 2014, **54**, 146.

